Scripta Materialia 169 (2019) 57–60

Contents lists available at ScienceDirect

Scripta Materialia

journal homepage: www.elsevier.com/locate/scriptamat

Shape memory effect in FeMnNiAl iron-based shape memory alloy

Wael Abuzaid [a,*], Huseyin Sehitoglu [b]

[a] Department of Mechanical Engineering, Materials Science and Engineering Research Institute, American University of Sharjah, PO Box 26666, Sharjah, United Arab Emirates
[b] Department of Mechanical Science and Engineering, University of Illinois at Urbana-Champaign, 1206 W. Green St., Urbana, IL 61801, USA

ARTICLE INFO

Article history:
Received 16 April 2019
Received in revised form 3 May 2019
Accepted 4 May 2019
Available online xxxx

Keywords:
Fe-based shape memory alloy
FeMnNiAl
Shape memory effect
Grain orientation
Martensite transformation

ABSTRACT

The development of Iron-based shape memory alloys holds significant promises for cost-sensitive applications. FeMnNiAl has been attracting increasing interest due to high levels of superelasticity across a wide range of temperatures (−196–300 °C). However, shape memory effect for this alloy system has not been demonstrated. In this study, the effect of aging treatments in inducing either shape memory or superelasticity is investigated. Shape memory strains of ≈ 4.5% are reported for polycrystalline $FeMn_{34}Ni_{7.5}Al_{13.5}$ (at.%). The observation of shape memory effect and the magnitude of recovery strains were dependent on aging conditions, crystal orientation, and deformation temperature.

The development and optimization of iron-based shape memory alloys (Fe-based SMA) is of great practical importance for cost-sensitive applications such as the construction industry [1,2]. This class of shape memory materials offers significant cost savings compared to NiTi and other commercially available SMA compositions. Many Fe-based SMAs have been proposed and shown to exhibit shape memory (SM) and superelastic properties (SE) [3–13]. Commercialization has been nevertheless very limited due to, in general, small levels of recovery strains, superelasticity being limited to low deformation temperatures, and relatively inferior fatigue properties. Recently, the FeMnNiAl Fe-based SMA has been receiving significant interest due to favorable superelastic properties across a wide range of temperatures extending from subzero to elevated temperatures [4,14–19]. With optimized grain size and precipitation content, superelastic strains as high as 10% have been reported. Despite significant progress in the understanding of this alloy system, efforts have so far been focused on the pseudoelastic behavior with no prior reports of shape memory effect in this Fe-based SMA. The ability to realize recovery strains through the SM effect in this alloy system is advantageous and enables the development of additional applications.

The stress induced martensitic transformation in FeMnNiAl SMA occurs between body-centered cubic (bcc) austenite phase and face-centered cubic (fcc) martensite phase [4]. To achieve good levels of recovery strains, large grain size and the introduction of coherent nano-precipitates in the austenite matrix are required [15,20]. Microstructures composed of large grains reduce the propensity for brittle martensite formation at grain boundaries which can promote grain boundary cracking and thus limit deformation and recovery levels. Such microstructures, typically referred to as bamboo structures having mm size grains, can be achieved through high-temperature cyclic heat treatment (*e.g.,* 800–1225 °C) which induce abnormal grain growth (AGG). Rapid cooling is typically required at the end of AGG treatments to retain the austenite bcc phase [21,22]. However, fast cooling rates (*i.e.,* through water quenching) can result in excessive stresses and grain boundary cracking. The precipitates size and volume fraction at the end of AGG heat treatment are not sufficient to achieve reversible thermoelastic martensitic transformation. Various studies have been dedicated to quantify and optimize the coherent precipitation content to achieve stable and full superelastic strain recovery [14,16,17]. The correct precipitate size is not only necessary for achieving thermoelastic transformation but is crucial for alloy stability by preventing undesirable room temperature aging effects [18]. There have been no studies, however, in which the correlation between different aging treatments and the tendency to exhibit shape memory effect has been subjected to investigation.

This study is dedicated to investigate the shape memory effect in FeMnNiAl Fe-based SMA. To the best of the authors' knowledge, there have been no previous reports of SM effect in this alloy system. The work provides a detailed quantitative assessment of the SM recovery strains in polycrystalline FeMnNiAl. The effect of aging treatments in inducing either SM or SE response is investigated. In addition, the impact of deformation temperature and crystal orientation on the SM recovery strains is explored. Overall, the work provides important insight into the potential use of the shape memory effect in this alloy system.

Polycrystalline $FeMn_{34}Ni_{7.5}Al_{13.5}$ (at.%) was investigated in the current study. Flat dog-bone tensile samples were electric discharge

* Corresponding author at: Department of Mechanical Engineering, American University of Sharjah, PO Box 26666, Sharjah, United Arab Emirates.
E-mail addresses: wabuzaid@aus.edu (W. Abuzaid), huseyin@illinois.edu (H. Sehitoglu).

https://doi.org/10.1016/j.scriptamat.2019.05.006
1359-6462/

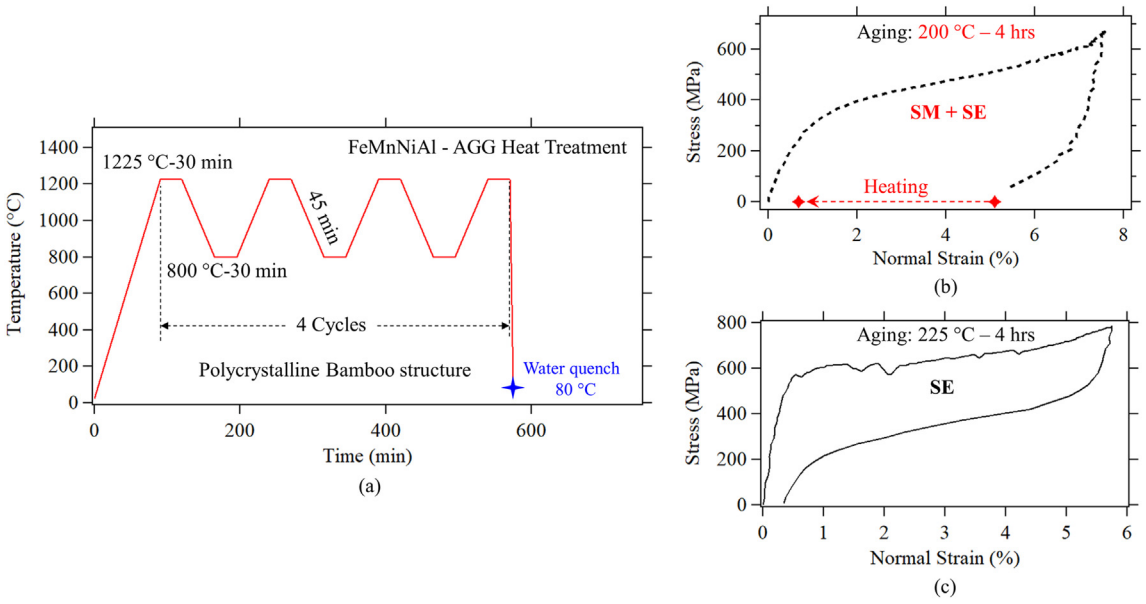

Fig. 1. (a) Cyclic heat treatment conditions for AGG. (b) Shape memory effect and superelasticity in FeMnNiAl with 200 °C aging temperature. (c) Full superelastic response with no shape memory strains for 225 °C aging temperature.

machined (EDM) with 3 × 1.5 mm^2 cross-sectional area and 10 mm gauge length. All specimens were encapsulated in quartz tubes (evacuated, and backfilled with Ar gas) prior to being subjected to cyclic heat treatment between 800 and 1225 °C with 30 min holding time at each extreme and 45 min ramping time. The process was repeated for 4 cycles as shown in Fig. 1a. At the end of the last holding time at 1225 °C, samples were quenched in 80 °C water. The resulting structure consisted of large grains with about 2 grains in the gauge section. Depending on the subsequent aging conditions, full superelasticity or primarily shape memory along with some SE strains were measured as shown in Fig. 1b–c. Results from 3 different sets of samples have shown full superelastic strains with 225 °C aging temperature and primarily SM strains at a slightly lower aging temperature (200 °C).

An example of a polycrystalline sample exhibiting superelasticity with 4 h aging at 225 °C is shown in Fig. 2a. The tension sample was subjected to multiple deformation cycles. A finite accumulation of irrecoverable (*i.e.*, permanent) strains was observed at the end of each loading cycle. Heating, in this case, did not induce any shape recovery and the specimen did not exhibit any significant shape memory effect. The gauge section of the specimen consisted of primarily two grains as shown in the grain orientation map in Fig. 2b. The strain contour plots presented in Fig. 2c point to the activation of a single martensite variant during transformation in Grain 1. We emphasize that the lack of full recovery, in this case, is associated with plasticity at the martensite boundary and not shape memory effect. Such degradation in superelastic strains, referred to as functional fatigue, is typical for FeMnNiAl SMA [15,23]. This aspect remains one of the major challenges in this alloy system, and in Fe-based SMAs in general.

A representative case showing shape memory response for FeMnNiAl is shown in Fig. 3. This sample was subjected to the exact same AGG heat treatment as the superelastic specimen discussed previously in Fig. 2, however, the aging temperature differed (200 °C compared to 225 °C). The gauge section of the specimen had two large grains as shown in the EBSD grain orientation map (Fig. 3b). The black

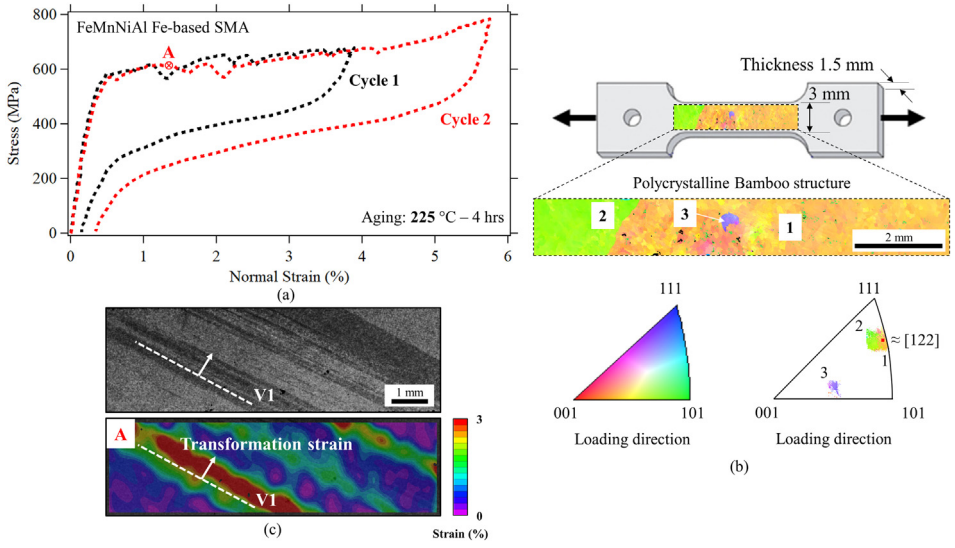

Fig. 2. (a) Stress-strain curves of superelastic FeMnNiAl tensile sample subjected to 2 deformation cycles. (b) Grain orientation map of the gauge section of the sample. The largest grain (grain 1) has a loading direction ≈ [122]. (c) Optical image and corresponding full-field strain contour plot of the vertical strain at point A shown in (a).

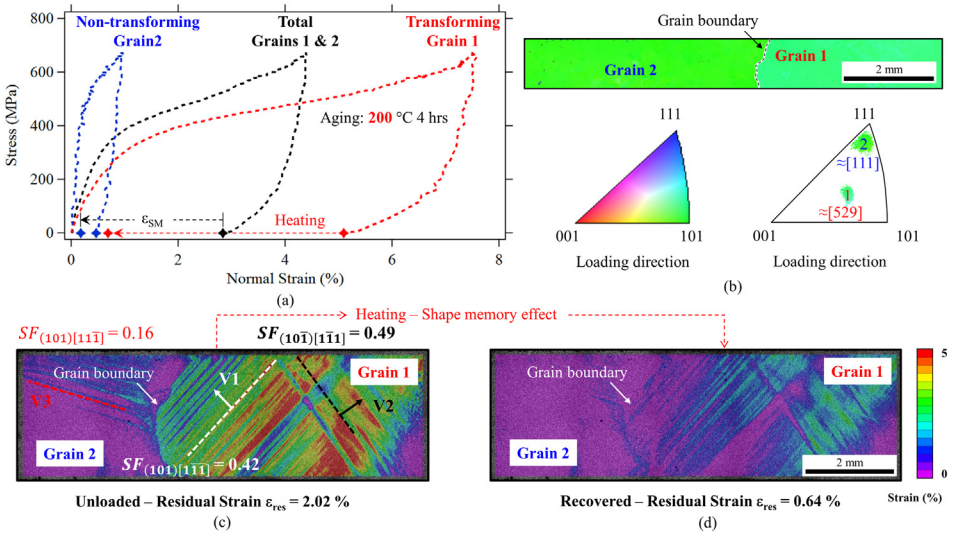

Fig. 3. (a) Stress-strain curves of FeMnNiAl tensile sample exhibiting superelasticity and shape memory properties. The different colored curves refer to the corresponding region used for strain calculation. (b) Grain orientation map of the gauge section of the sample. High-resolution strain contour plot showing the residual vertical strain following unloading (c) and after temperature-induced shape recovery (d).

colored stress-strain curve in Fig. 3a was constructed using the average DIC strain field in the entire gauge section including both grains (Grains 1 & 2). Clearly, the average response points to limited levels of superelastic strain recovery upon unloading and shape memory strains of ≈2.5% following heating. The deformation was, however, not homogeneous and highly localized in Grain 1 as shown in the high-resolution strain contour plot in Fig. 3c. The second grain in the gauge section (*i.e.*, Grain 2) experienced limited levels of transformation. This dissimilar response, induced by the difference in grain orientation, is clearly observed from the local stress-strain curves generated for both grains, separately. The Grain 1 stress-strain curve (red curve in Fig. 3a) shows applied strains reaching 8% with shape memory strains of ≈4.5%. The deformation levels for Grain 2 did not exceed 1% and were significantly less than Grain 1. A summary of all the measured strain magnitudes, total, Grain 1, and Grain 2 is presented in Table 1.

To shed further insight into the source of the deformation heterogeneity, both grain orientations and the high-resolution DIC results were utilized to identify potential variant activation. Habit planes along the {110} have been previously observed for single crystalline FeMnNiAl [24]. All the observed strain bands (traces) in the strain contour plot shown in Fig. 3c were identified to coincide with one of the {110} planes. Based on resolved shear stress calculation (*i.e.*, Schmid factor), with shear directions along the ⟨111⟩ crystallographic directions, the two activated variants in Grain 1, V1 and V2, were the ones having the highest Schmid factors magnitudes compared to all other potential variants (0.49 and 0.42). In comparison, the maximum Schmid factor in Grain 2 was 0.37 which explains the relatively lower levels of deformations. The activated variant in Grain 2 (marked as V3 in Fig. 3c), was not, however, the variant with the maximum Schmid factor. The activation of this variant took place in the vicinity of the grain boundary (Grain 2 side) and is expected to have been induced by the high localized stress generated by transformation in the neighboring grain (*i.e.*, V1 grain boundary interaction). In addition to the previous analysis, we note that theoretical calculations of the transformation strains identify the [111] orientation, which is the loading direction in the relatively non-transforming Grain 2, as the orientation having the lowest magnitude of transformation strain [24,25]. This further explains the inferior levels of transformation in Grain 2 compared to Grain 1 which has a relatively favorable orientation.

Heat treatments optimized for superelasticity in FeMnNiAl Fe-based SMA have demonstrated high levels of superelastic strains across a wide range of temperatures (−193–300 °C). The measured transformation stress levels exhibit small temperature dependence (≈0.5 MPa/°C), compared to other SMAs, which is very attractive from a practical perspective. With aging conditions resulting in partial superelasticity and shape memory effect upon heating (*i.e.*, the 200 °C aging treatment as shown in this work), the effect of deformation temperature is not clear in this case and requires further investigation. Identification of phase transformation temperatures would be advantageous in addressing this issue, in particular, the martensite start (M_s) and austenite finish temperatures (A_f), however, such measurements remain a challenge for FeMnNiAl and Fe-based SMAs in general. To further investigate the effect of deformation temperature on the response of samples aged for shape memory behavior, two samples were deformed at 25 °C and 180 °C to similar strain levels (≈4.5% applied strain). The comparison between the two samples is provided in Fig. 4. Clearly, with temperature increase, the magnitude of superelastic strains increased which would consequently result in lower levels of shape memory strains. A summary of the resulting strain magnitudes is presented in Table 2. As the shape memory effect relates to the presence of martensite phase prior to deformation, the reduction in shape memory strains, and amplification of superelastic strains, with deformation temperature increase suggests a drop in the martensite volume fraction. Such a drop can occur if the austenite finish temperature is higher than 25 °C and

Table 1
Summary of the applied, superelastic, shape memory, and residual strain magnitudes for the specimen discussed in Fig. 3.

Region	Max applied strain ε (%)	Recovered strain ε_{SE} (%)	Shape memory strain ε_{SM} (%)	Residual strain ε_{res} (%)
Total gauge section (Grains 1 & 2)	4.4	1.4	2.5	0.5
Grain 1 Loading direction ≈ [529]	7.6	2.2	**4.7**	0.7
Grain 2 Loading direction ≈ [111]	1.0	0.5	0.3	0.2

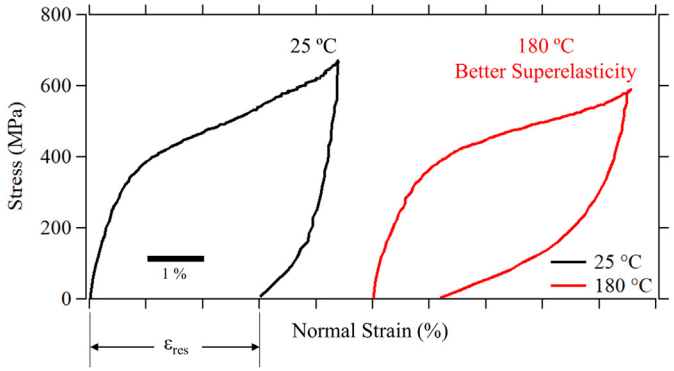

Fig. 4. Stress-strain curves of FeMnNiAl tensile sample exhibiting superelasticity and shape memory properties at different deformation temperatures.

potentially even higher than the aging temperature of 200 °C. In addition, the presence of martensite during room temperature deformation can be induced by a martensite start temperature above 25 °C. The identification of phase transformation temperatures using differential scanning calorimetry (DSC) is not feasible in this Fe-based SMA. Despite some efforts to identify transformation temperatures in FeMnNiAl SMA, for example, M_s using dilatometry measurements [17], electric resistivity measurements [26], and magnetization measurements [4,19,27], a comprehensive quantitative assessment of transformation temperatures remains a challenge. In addition, heat treatment conditions and their influence on the martensite/austenite volume fractions still require further investigation. Such efforts are well motivated as they are crucial for proper control and customization of either the SE or SM response in FeMnNiAl.

It's important to note that despite the clear ability to achieve shape memory effect in FeMnNiAl with SM strains as high as 4.7% as shown in this work, limited levels of superelasticity was still detectable. Efforts to optimize aging conditions for complete and full SM strain recovery were attempted, however, with limited success. With further reduction in aging time or temperature, which has an inverse relation with precipitates size and volume fraction, deformation was primarily accommodated through plastic slip with limited SE or SM strains. The conditions reports in this work (200 °C for 4 h.) resulted in the highest magnitudes of SM strains, however, further improvements can potentially be gained through further optimization and fine-tuning of aging conditions. Another aspect that would help optimize the SM strain magnitudes is proper control of grain orientation. In the results presented in Fig. 3, the grain with loading along the [529] orientation achieved significantly higher SM strains compared to the other grain with loading along the [111] direction (4.7 compared to 0.3%, respectively). Loading along the [001] should theoretically provide higher magnitudes of transformation strains. However, the currently adopted AGG heat treatment procedures do not allow for proper control and selective growth of specific orientations and/or texturing.

The shape memory effect and SM strain magnitudes reported in this work decreased once the deformation temperature was increased from around 25 to 180 °C. The achieved levels of SM strains will potentially improve at lower deformation temperatures, however, high-temperature SM effect will obviously be limited. Extending the SM range will require increasing the M_s temperature. A clear path to accomplish this task is not feasible yet based on the current understanding of heat treatment and aging effects. In fact, previous works have shown that the M_s temperature attained its highest value prior to aging and decreased after any aging treatments [17,26]. It should be noted that samples deformed following AGG treatments only (*i.e.*, no aging, potentially the highest M_s temperature) deformed plastically without exhibiting any SE or SM strains. Despite this limitation, various applications can still be envisioned for FeMnNiAl utilizing the shape memory effect at room temperature, and below.

Table 2
Summary of the applied, residual, and superelastic strain magnitudes for the specimen discussed in Fig. 4.

Deformation temperature (°C)	Max applied strain ε (%)	Residual strain ε_{res} (%)	Recovered strain ε_{SE} (%)
25	4.4	3.0	1.4
180	4.6	1.2	3.4

In summary, the work has investigated the effect of aging conditions on the shape memory properties of FeMnNiAl Fe-based SMA. With proper selection of aging temperature and time, the alloy can be tailored to exhibit shape memory effect at room temperature. The shape memory strains were accommodated by multiple martensite variants having the highest Schmid factors. Grains with unfavorable orientations, based on resolved shear stress, exhibited limited levels of transformation strains leading to highly heterogeneous deformation fields. At elevated temperatures, superelastic strains increased at the expense of shape memory strains. This was attributed to low M_s temperature and a reduction in martensite volume fraction.

Acknowledgments

The work has been partially supported by an NSF DMR Grant 1709515 which is gratefully acknowledged. The corresponding author would like to acknowledge the partial financial support from the American University of Sharjah (EFRG18-MSE-CEN-22).

References

[1] T. Maruyama, H. Kubo, Shape Mem. Superelastic Alloy. (2011) 141–159.
[2] A. Cladera, B. Weber, C. Leinenbach, C. Czaderski, M. Shahverdi, M. Motavalli, Constr. Build. Mater. 63 (2014) 281–293.
[3] T. Maki, K. Kobayashi, M. Minato, I. Tamura, Scr. Metall. 18 (1984) 1105–1109.
[4] T. Omori, K. Ando, M. Okano, X. Xu, Y. Tanaka, I. Ohnuma, R. Kainuma, K. Ishida, Science 333 (80) (2011) 68–71.
[5] Y.N. Koval, V.V. Kokorin, L.G. Khandros, Phys. Met. Metallogr. 48 (1979) 162–164.
[6] Y.I. Chumlyakov, I.V. Kireeva, V.V. Poklonov, Z.V. Pobedennaya, I. Karaman, Tech. Phys. Lett. 40 (2014) 747–750.
[7] Y.I. Chumlyakov, I.V. Kireeva, O.A. Kuts, Y.N. Platonova, V.V. Poklonov, I.V. Kukshauzen, D.A. Kukshauzen, M.Y. Panchenko, K.A. Reunova, Russ. Phys. J. 58 (2016) 1549–1556.
[8] T. Omori, R. Kainuma, Shape Mem. Superelasticity 3 (2017) 322–334.
[9] E. Hornbogen, N. Jost, Le J. Phys. IV 01 (1991) C4-199-C4-210.
[10] H. Sehitoglu, I. Karaman, X. Zhang, Y. Chumlyakov, H. Maier, Scr. Mater. 44 (2001) 779–784.
[11] H. Sehitoglu, C. Efstathiou, H.J. Maier, Y. Chumlyakov, J. Magn. Magn. Mater. 292 (2005) 89–99.
[12] J. Ma, B. Kockar, A. Evirgen, I. Karaman, Z.P. Luo, Y.I. Chumlyakov, Acta Mater. 60 (2012) 2186–2195.
[13] W. Abuzaid, H. Sehitoglu, Mater. Des. 160 (2018) 642–651.
[14] L.W. Tseng, J. Ma, B.C. Hornbuckle, I. Karaman, G.B. Thompson, Z.P. Luo, Y.I. Chumlyakov, Acta Mater. 97 (2015) 234–244.
[15] M. Vollmer, P. Krooß, M.J. Kriegel, V. Klemm, C. Somsen, H. Ozcan, I. Karaman, A. Weidner, D. Rafaja, H. Biermann, T. Niendorf, Scr. Mater. 114 (2016) 156–160.
[16] H. Ozcan, J. Ma, S.J. Wang, I. Karaman, Y. Chumlyakov, J. Brown, R.D. Noebe, Scr. Mater. 134 (2017) 66–70.
[17] P. La Roca, A. Baruj, C.E. Sobrero, J.A. Malarría, M. Sade, J. Alloys Compd. 708 (2017) 422–427.
[18] M. Vollmer, M.J. Kriegel, A. Walnsch, V. Klemm, A. Leineweber, T. Niendorf, Scr. Mater. 162 (2019) 442–446.
[19] J. Xia, X. Xu, A. Miyake, Y. Kimura, T. Omori, M. Tokunaga, R. Kainuma, Shape Mem. Superelasticity 3 (2017) 467–475.
[20] T. Omori, H. Iwaizako, R. Kainuma, Mater. Des. 101 (2016) 263–269.
[21] M. Vollmer, C. Segel, P. Krooß, J. Günther, L.W. Tseng, I. Karaman, A. Weidner, H. Biermann, T. Niendorf, Scr. Mater. 108 (2015) 23–26.
[22] L.W. Tseng, J. Ma, M. Vollmer, P. Krooß, T. Niendorf, I. Karaman, Scr. Mater. 125 (2016) 68–72.
[23] M. Vollmer, M.J. Kriegel, P. Krooß, S. Martin, V. Klemm, A. Weidner, Y. Chumlyakov, H. Biermann, D. Rafaja, T. Niendorf, Shape Mem. Superelasticity 3 (2017) 335–346.
[24] L.W. Tseng, J. Ma, S.J. Wang, I. Karaman, Y.I. Chumlyakov, Scr. Mater. 116 (2016) 147–151.
[25] A. Ojha, H. Sehitoglu, Int. J. Plast. 86 (2016) 93–111.
[26] P. La Roca, J. Medina, C.E. Sobrero, M. Avalos, J.A. Malarria, A. Baruj, M. Sade, MATEC Web Conf. 33 (2015), 04005.
[27] L.W. Tseng, J. Ma, S.J. Wang, I. Karaman, M. Kaya, Z.P. Luo, Y.I. Chumlyakov, Acta Mater. 89 (2015) 374–383.